Journal of Radiation Research, 2014, 55, 191–199
doi: 10.1093/jrr/rrt100 Advance Access Publication 26 August 2013

Evaluation of imaging performance of megavoltage cone-beam CT over an extended period

Iori SUMIDA[1,2,*], Hajime YAMAGUCHI[2], Hisao KIZAKI[2], Yuji YAMADA[2], Masahiko KOIZUMI[3], Yasuo YOSHIOKA[3], Kazuhiko OGAWA[3], Naoya KAKIMOTO[1], Shumei MURAKAMI[1] and Souhei FURUKAWA[1]

[1]Department of Oral and Maxillofacial Radiology, Osaka University Graduate School of Dentistry, 1-8 Yamada-oka, Suita, Osaka, 565-0871, Japan
[2]Department of Radiation Oncology, NTT West Osaka Hospital, 2-6-40 Karasugatsuji, Tennoji-ku, Osaka, 543-8922, Japan
[3]Department of Radiation Oncology, Osaka University Graduate School of Medicine, 2-2 Yamada-oka, Suita, Osaka, 565-0871, Japan
*Corresponding author. Department of Oral and Maxillofacial Radiology, Osaka University Graduate School of Dentistry, 1–8 Yamada-oka, Suita, Osaka, 565-0871 Japan. Tel: +81-6-6879-2967; Fax: +81-6-6879-2970; Email: isumida@dent.osaka-u.ac.jp

(Received 26 November 2012; revised 1 July 2013; accepted 18 July 2013)

A linear accelerator vendor and the AAPM TG-142 report propose that quality assurance testing for image-guided devices such megavoltage cone-beam CT (MV-CBCT) be conducted on a monthly basis. In clinical settings, however, unpredictable errors such as image artifacts can occur even when quality assurance results performed at this frequency are within tolerance limits. Here, we evaluated the imaging performance of MV-CBCT on a weekly basis for ~1 year using a Siemens ONCOR machine with a 6-MV X-ray and an image-quality phantom. Image acquisition was undertaken using 15 monitor units. Geometric distortion was evaluated with beads evenly distributed in the phantom, and the results were compared with the expected position in three dimensions. Image-quality characteristics of the system were measured and assessed qualitatively and quantitatively, including image noise and uniformity, low-contrast resolution, high-contrast resolution and spatial resolution. All evaluations were performed 100 times each. For geometric distortion, deviation between the measured and expected values was within the tolerance limit of 2 mm. However, a subtle systematic error was found which meant that the phantom was rotated slightly in a clockwise manner, possibly due to geometry calibration of the MV-CBCT system. Regarding image noise and uniformity, two incidents over tolerance occurred in 100 measurements. This phenomenon disappeared after dose calibration of beam output for MV-CBCT. In contrast, all results for low-contrast resolution, high-contrast resolution and spatial resolution were within their respective tolerances.

Keywords: Cone-beam CT; QA; image-guided radiation therapy; IGRT; tolerance; calibration

INTRODUCTION

Image-guided radiation therapy (IGRT) during patient set-up prior to treatment delivery allows the patient to be positioned as closely as possible to the expected irradiation position. Several recent IGRT techniques include fan-beam CT [1–3], CT-on-rails [4], cone-beam CT (CBCT) [5–6], electronic portal imaging device (EPID) [7], ultrasound system [8] and infrared marker [9]. The first four of these techniques use X-rays in kilovoltage or megavoltage beam quality. Depending on beam quality, however, these techniques may include features such as image contrast between bony structures and soft tissues, and the presence metallic artifacts. Correct placement of the patient requires assurance of the performance of imaging devices in terms of both image quality and the lack of geometrical distortion related to the treatment room coordinates. These items should be confirmed stable within the institution's tolerance limits.

Our department uses a megavoltage CBCT (MV-CBCT) for IGRT. MV-CBCT uses the same X-ray source and gantry as those used for treatment. It also uses the same EPID as for 2D imaging and thus eliminates the requirement for isocenter matching calibration. The linear accelerator (linac) vendor has proposed quality assurance (QA) instructions for MV-CBCT that should be performed on a monthly basis (referred to in Siemens MVision Physicist Self-Led Training). QA frequency has also been proposed in the American Association of Physicists in Medicine Task Group 142 report [10]. This instruction includes a check of image quality and geometric distortion in the three dimensions of lateral, longitudinal and vertical. The vendor also provides users with an original QA phantom for performing these tests. Based on the vendor instructions, the measurement protocol is defined with 15 monitor units (MU) with low-energy photons for irradiation and the use of a filter named 'smoothing head and neck'. A smoothing filter is applied to the reconstructed images to correct for the cupping effect due to the large amount of scatter inherent in the large field sizes in cone-beam geometry [11]. This filter has two naming options, 'pelvis' or 'head and neck', which corrects the cupping effect based on the size of the respective anatomical site, and 3 (head and neck region) or 5 MU (abdominal region) are used for image guidance in clinical settings to minimize the absorbed dose the patient receives during visualization [12, 13]. Even when the results of monthly QA performed with 15 MU are within tolerance, occasional errors such as streak artifacts, tyre-track artifacts, image non-uniformity, and undesirable contrast resolution have been noted in clinical use. The high-quality protocol suggested by the vendor for MV-CBCT at the linac for image quality assessment does not reflect the clinically recommended scan protocol, and subtle changes in imaging performance may occur within the 1-month testing period. In addition, if image quality does in fact decrease with time, a reduction in positioning or registration accuracy can be expected.

Here, to verify and track possible changes in QA results over periods of as long as one year, we performed the vendor-proposed QA on a weekly rather than monthly basis.

MATERIALS AND METHODS

Irradiation

An X-ray beam from an ONCOR Impression Plus dual photon energy linear accelerator (6 MV and 10 MV; Siemens Medical Systems, Erlangen, Germany) was used. Portal images were acquired with a Siemens OPTIVUE 1000 EPID (Siemens Medical Systems). The portal imager has matrices of 1024 × 1024 pixels with a physical size of 0.40 mm, giving an active area of 41 × 41 cm^2. A 3-mm copper plate overlays the sensitive layer of the EPID to remove low-energy photons; immediately beneath the copper plate is a scintillating layer of phosphor to transform incoming X-rays to visible photons, and then a pixel array implanted on the amorphous-Si panel to capture visible photons and convert them to electric charges. The charge signals are then read out and digitized by a 16-bit analog-to-digital converter. Source to image distance (SID) is changeable between 110 cm and 160 cm. QA measurements for MV-CBCT were rotational irradiation, which started at a gantry angle of 270° to 110° at a fixed SID of 145 cm with a 27.4 cm × 27.4 cm field size and low energy photons of 6 MV. SID was defined by the vendor.

Following insertion of the orthogonal tungsten wires (which are named the XRETIC plate and are matched to the mechanical isocenter) into the shadow tray, the Siemens image quality phantom (called the EMMA phantom, Siemens Medical Systems) was manually set to the isocenter using the wire shadow at gantry angles of 0°, 90° and 270° by matching the projection of the two orthogonal metal wires of the XRETIC plate with the reference lines of the phantom in the anterior and two lateral directions. After MV-CBCT irradiation, the system automatically reconstructs the CBCT image in a slice thickness of 1 mm and 256 × 256 matrices with filtered correction of cupping artifacts named 'smoothing head and neck', as described above. Voxel size was 1.07 mm × 1.07 mm × 1.00 mm in the lateral, vertical and longitudinal directions, respectively. Reconstructed image sets of a total of 274 slices were outputted and imported into our in-house software developed using CodeGear Delphi 2007. MV-CBCT imaging by the phantom analysis described below was performed 100 times per week for ~ 1 year. Evaluation of image quality with regard to low-contrast resolution, high-contrast resolution, and contrast-to-noise ratio was done by displaying transverse slices using a 5-mm multiple plane reconstruction view on the in-house software to reduce noise. This method is also based on the vendor's protocol.

Phantom analysis

The specification for the EMMA phantom is shown in Fig. 1. The EMMA phantom has three sets, each of four beads, that are used to check geometric distortion in three dimensions. The beads are distributed evenly around the circumference of

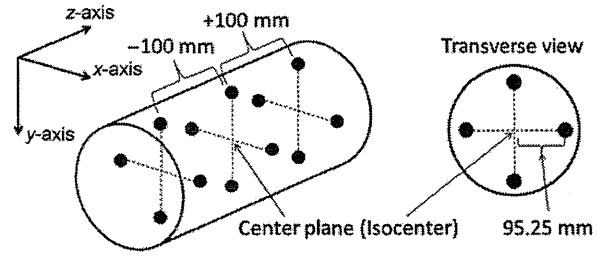

Fig. 1. The EMMA phantom geometry and bead configuration in 3D and transverse views. Four beads are evenly separated from the center of the phantom by 95.25 mm in transverse view. Transverse planes are located at intervals of 100 mm along the *z*-axis.

the phantom with z coordinates of 100 mm, 0 mm and – 100 mm for the superior, center and inferior slices, respectively. The four beads in each slice are located at the 3, 6, 9 and 12 o'clock positions, respectively. Each of the four beads is separated from the center of the phantom by +95.25 mm.

For the geometric distortion check, a reference point was manually placed at the center of each bead in the MV-CBCT image of the phantom using the in-house software, and then the position was compared with that of the nominal position. The deviation from the nominal position was measured for each bead. The tolerance level of 2 mm was defined by the vendor. Minimum pixel resolution for analysis in the in-house software was 0.27 mm in the lateral and vertical axes, and 0.23 mm in the longitudinal axis.

With regard to checking image quality, the EMMA phantom has a solid region that consists of four sections, namely: (a) a solid water section, (b) a low-contrast resolution section, (c) a spatial resolution section, and (d) a high-contrast resolution section. The solid region of the EMMA phantom is shown in Fig. 2.

Section (a) is a 40-mm uniform solid water cylinder that is used to check image noise and the uniformity of pixel values. On the central slice of this section, five circular regions of interest (ROIs) were automatically drawn on the image; one in the center and four in the periphery at the 3, 6, 9 and 12 o'clock positions at an equidistance of 69.6 mm from the center of the phantom, as shown in Fig. 3. The distance of 69.6 mm was determined to be suitably close to the edge of the phantom and was used for all analyses. The diameter of the ROI was 2 cm.

The mean pixel value and standard deviation for each ROI were calculated, and the pixel value was then compared with the vendor specification. Expected results for 6-MV acquisitions were as follows: the center ROI, which is numbered 2, should have (i) a standard deviation between +26 and +42, and (ii) a mean value of pixels between – 30 and +42. The difference between the mean pixel value of each peripheral ROI and the mean pixel value of the central ROI was calculated, and it was verified that the difference fell within the expected range of – 80 to +80. Image reconstruction artifacts due to dead pixels or wrong gantry rotation speed were also visually checked on each slice of this section.

Sections (b) and (d), which contain inserts of different material rods with various diameters inside a solid water background, are shown in Fig. 4.

The physical density and relative electron density of each material with respect to the background are presented in Table 1.

Low-contrast resolution was qualitatively checked by adjusting the window level and window width to preset values, and by counting the number of inserts of each material that were visible on the image. After the set of ROI included all inserts in each slice, the mean, maximum and minimum pixel values were calculated. The mean pixel value was used for the window level, and the difference between the minimum and maximum values was used for the window width in order to define the preset values for visual evaluation. Table 2 lists the circles that should be visible in each of the eight groups in sections (b) and (d) under image acquisition at 6 MV.

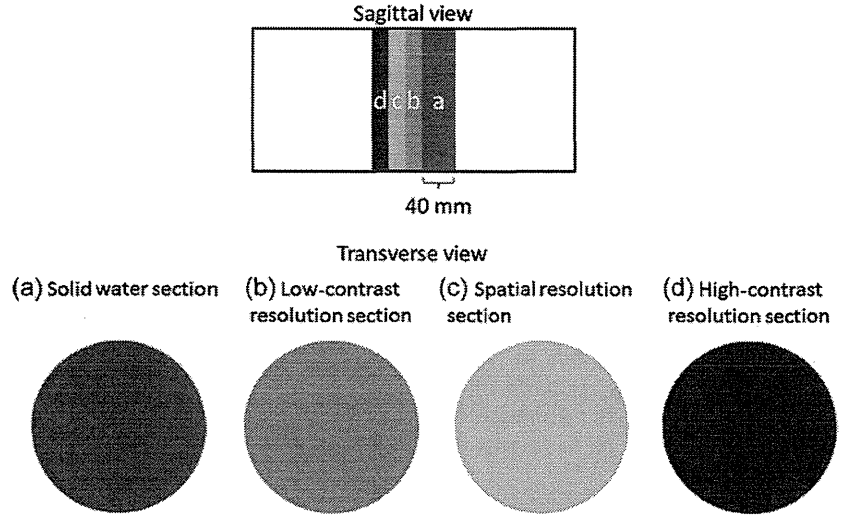

Fig. 2. Four solid sections of the EMMA phantom in sagittal and transverse view. These sections in transverse view consist of (**a**) solid water section, (**b**) low-contrast resolution section, (**c**) spatial resolution section, and (**d**) high-contrast resolution section, respectively.

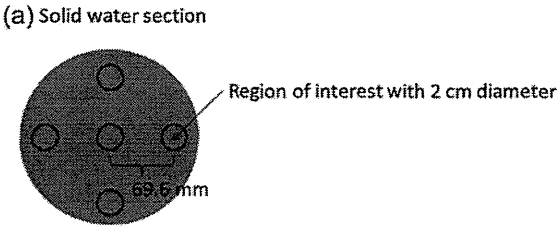

Fig. 3. Five ROIs in the solid water section. Four peripheral ROIs are placed, evenly separated by 69.6 mm from the center of the phantom. The diameter of each ROI is 2 cm.

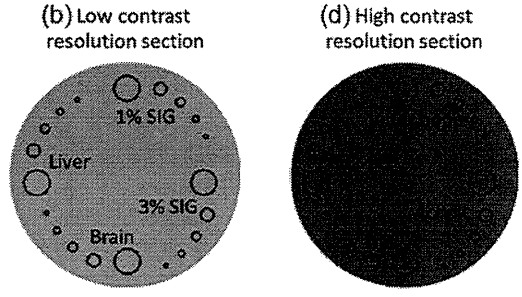

Fig. 4. Low-contrast resolution section (**b**), and high-contrast section (**d**) of the EMMA phantom. Each section has inserts of four different materials, namely (b) brain, liver, 1% SIG, and 3% SIG, and (d) air, CB2-50%, inner bone, and acrylic. The diameter of the five rods for each material is 2, 1, 0.7, 0.5 and 0.3 cm, respectively. SIG means standard imaging grade, which is the background material. CB2-50% means $CaCO_3$.

Different material rods in section (d) were also used to calculate the contrast-to-noise ratios (*CNR*) as presented by Gayou *et al.* [14]. The equation for *CNR* was:

$$CNR = \frac{|S - S_{BG}|}{\sigma}, \quad (1)$$

where S and S_{BG} are the mean pixel values in an insert and the background region surrounding the insert, respectively, and σ is the average standard deviation of the pixel value in the insert and the background. Since this analysis was a quantitative evaluation and the position of each rod and of the background region was clearly defined, each ROI of 2-cm diameter was automatically set to its position in the same manner as in pixel uniformity analysis, as shown in Fig. 3. With regard to the background region after the image was rotated counterclockwise 20°, the ROI at the same position was used for calculation.

Section (c) was used to analyze the spatial resolution of the image. This section contained 11 bar groups, each group of which contained 5 bars, arranged so that each group had a different resolution, as shown in Fig. 5.

Table 1. Physical density and relative electron density of materials with respect to background

Section	Material	Physical density (g/cm^3)	Electron density
ii	Brain	1.05	1.04
ii	Liver	1.09	1.06
ii	1% SIG	1.03	1.00
ii	3% SIG	1.05	1.02
iv	Air	0.00	0.00
iv	CB2-50%	1.56	1.47
iv	Inner bone	1.14	1.08
iv	Acrylic	1.18	1.16

SIG = standard imaging grade of background material, CB2-50%, $CaCO_3$.

Table 2. Number of rods that should be visible in each of the eight groups in 6-MV image acquisition

Section	Material	Visible rods count
ii	Brain	1
ii	Liver	2
ii	1% SIG	0
ii	3% SIG	0
iv	Air	5
iv	CB2-50%	5
iv	Inner bone	4
iv	Acrylic	4

SIG = standard imaging grade of background material, CB2-50%, $CaCO_3$.

Table 3 shows the specification of the chart for each bar group. This is a qualitative analysis based on the number of bars that are visible on the image in which we determine how many groups (each with five line pairs) are visible. The expected results for this test using 6-MV image acquisitions are that the largest to the sixth-largest line group (corresponding to 0.30 LP/mm); in other words, the Nyquist frequency was calculated as 1 divided by twice the sampling frequency of 1.67 mm should be visible with all five dark lines distinctly visible, whereas lines 7–11 should not be resolvable, in accordance with the limitations of current imaging technology.

RESULTS

Figure 6 shows positional errors of the measured positions of the 12 beads with respect to the expected positions from 100 measurements. All beads were within the recommended ±2 mm position precision in all three directions. For the x-axis,

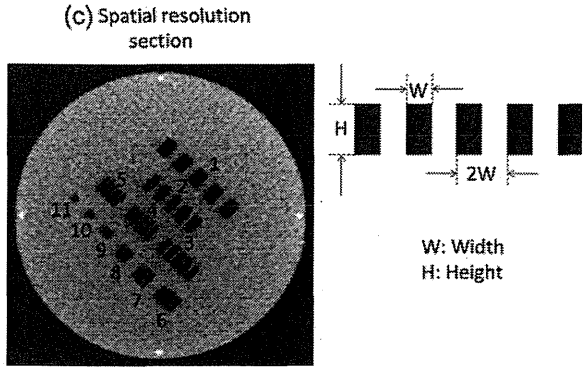

Fig. 5. Spatial resolution section (c) of the EMMA phantom containing 11 bar groups with different numbers of line pairs per millimeter. Width of each line pair is labeled 'W' and the height is labeled 'H'.

Table 3. Specification of the chart for each bar group and Nyquist frequency in line pairs per millimeter calculated by width

Bar group	W (mm)	H (mm)	LP/mm
1	7.5	12.0	0.067
2	5.0	12.0	0.1
3	3.3	12.0	0.15
4	2.5	12.0	0.2
5	2.0	12.0	0.25
6	1.67	12.0	0.3
7	1.25	12.0	0.4
8	1.0	10.0	0.5
9	0.83	6.6	0.6
10	0.62	5.0	0.8
11	0.5	4.5	1.0

W = width, H = height.

positional errors at 12 o'clock in all planes (head 10 cm, center, and foot 10 cm) were positive values, while those at 6 o'clock in all planes were negative. For the *y*-axis, positional errors at 3 o'clock in all planes were positive values, while those at 9 o'clock in all planes were negative. This pattern suggests that placement of the EMMA phantom might have been biased slightly toward the clockwise direction in each manual setup. For the *z*- axis, positional errors in the two center and head 10-cm planes were negative values, while those in the foot 10-cm plane were positive. However, uncertainties in the subjective, user-dependent placement of the reference point at the center of the bead might have contributed to these variations.

Figure 7 shows the mean pixel value and one standard deviation for the ROI at the center position, and the difference pixel value at each ROI of 3, 6, 9 and 12 o'clock compared with the center position from 100 measurements. The measured values of two of the 100 measurements for mean pixel value were outside the range of – 30 to +42 (shown in black arrows), at – 40 and +203. All values were within tolerance after the adjustment in beam output for cone-beam CT acquisition. Other values at the second black arrow for SD, 3, 6, 9 and 12 o'clock were also outside the tolerance range. After the adjustment of beam output for cone-beam CT acquisition, these values were within the tolerance range. Apart from these two occurrences, other pixel values for the mean and SD at each ROI position were within the tolerance range.

Figure 8 shows the visible rod counts at the low- and high-contrast resolution sections for various materials from 100 measurements. For the low-contrast resolution section, all materials at up to the diameter specified by the vendor were visible. For the liver rod material, 95 of 100 measurements were more visible than expected, as were 83 of 100 measurements for the brain. For the high-contrast resolution section, all materials with up to the specified diameter by the vendor were also visible.

Figure 9 shows the *CNR* for the three different material rods of CB2-50%, inner bone, and acrylic from 100 measurements. The *CNR* value of CB2-50% was 15.9 ± 0.8 (mean ± SD), which was remarkably higher than those of inner bone (2.5 ± 0.2) and acrylic (3.7 ± 0.2) considering the electron density of each material.

For the evaluation of spatial resolution section by visual inspection, bars in Group 6, that is up to 0.3 LP/mm, were clearly visible for 100 measurements.

DISCUSSION

Imaging performance of MV-CBCT was evaluated with regard to geometrical distortion and image quality for ~ 1 year using 100 measurements. Although the vendor has recommended that the QA used for this study should be performed every month, we changed this frequency to a weekly basis in order to identify subtle changes in characteristics, such as in geometrical distortion and imaging quality, and to evaluate whether the 1-month frequency was valid. In this regard, the AAPM TG-147 report also states that the frequency of the test may be increased upon vendor recommendation [15]. For geometrical distortion, relative position errors of all beads were within the 2-mm tolerance specified by the vendor. Figure 10 shows a vector diagram of positional errors in the central plane in axial view. We performed the QA test 100 times over a period of ~ 1 year, but the tendency identified in Fig. 10 was maintained throughout the test period. The values in Fig. 10 represent the mean translational errors in millimeters for 100 measurements. Although the error value was small, with a measurement uncertainty of

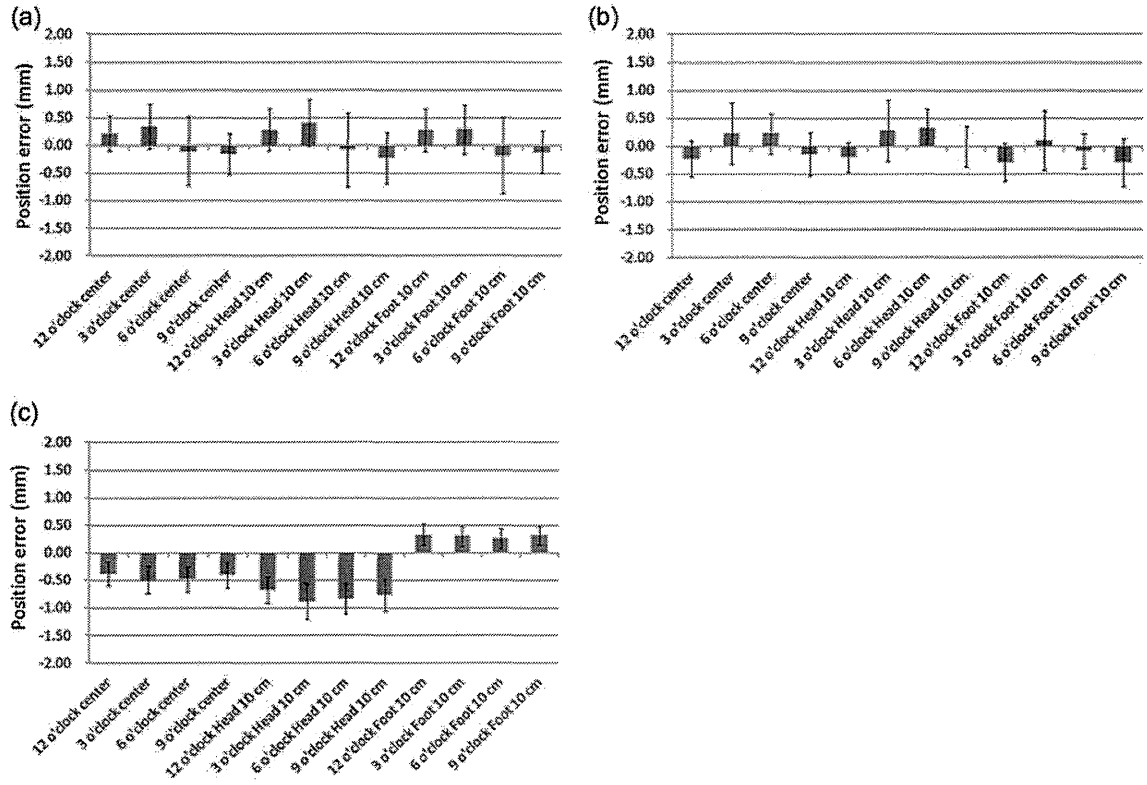

Fig. 6. Positional errors of measured positions of the 12 beads with respect to the expected positions from 100 measurements in the x, y and z axes. The vertical axes show the positional errors of relative lateral (**a**: x-axis), vertical (**b**: y-axis), and longitudinal (**c**: z-axis) measured positions of the 12 beads embedded in the EMMA phantom, with respect to their nominal values at their own bead positions. Each bar presents the mean value from 100 measurements, and the error bar means one standard deviation.

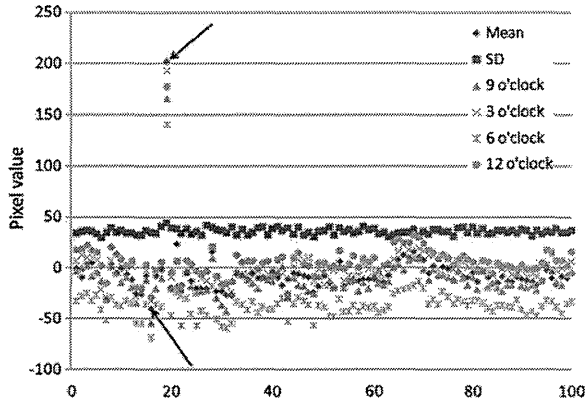

Fig. 7. Mean pixel value and 1 SD for the ROI at the center position, and difference in pixel value at each ROI of 3, 6, 9 and 12 o'clock compared with the center position from 100 measurements. The vertical axis shows the pixel value of the mean and 1 SD of the center ROI and that of the ROI at 3, 6, 9 and 12 o'clock from 100 measurements. SD means one standard deviation. The two black arrows indicate measurements in which the pixel values were out of tolerance.

0.14 mm (calculated from the minimum resolution of 0.27 mm divided by 2), vector sums at the four positions of 3, 6, 9 and 12 o'clock might indicate a tendency to rotational error of $0.11 \pm 0.22°$ (mean $\pm$ SD) from the 100 measurements with respect to the z-axis in the clockwise direction. Figure 11 shows axial and coronal views of a bucket filled with water taken by MV-CBCT. We confirmed that the water plane was slightly tilted by 0.27° in the clockwise direction on the axial image, and that the image was asymmetric in the left-to-right direction in the coronal image. The water plane should clearly be parallel to a floor, according to gravity. We interpret this strange phenomenon to mean that the geometry calibration for MV-CBCT acquisition is not perfect. Pouliot *et al.* described the geometry calibration procedure in detail [5]. After the geometry phantom was carefully aligned around the machine isocenter, an image was acquired for each of the 200 gantry angles of the cone beam arc. The lookup tables, which are 4×4 matrices, consist of the rotation and translation for each projection image, and are automatically created to correct errors in the vertical and horizontal scale and skew of the detector that can be caused

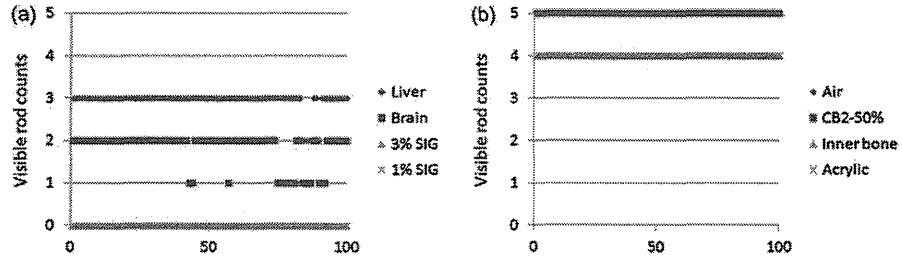

Fig. 8. Visible rod counts at low- and high-contrast resolution sections for various materials from 100 measurements. The vertical axis shows the visible rod counts for each material at the (**a**) low-contrast resolution section, and (**b**) high-contrast resolution section from 100 measurements. For both contrast sections the visible rod counts were within the tolerance specified by the vendor.

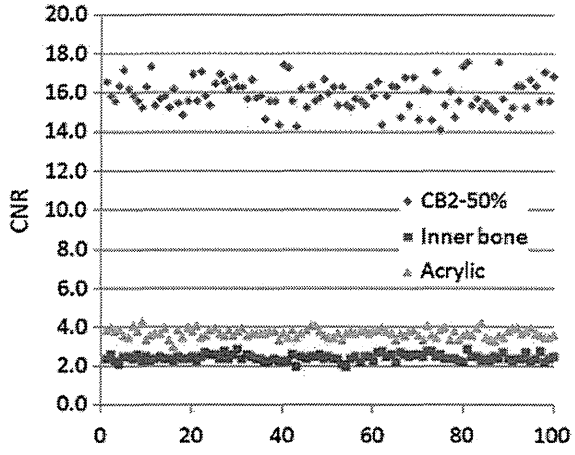

Fig. 9. Contrast-to-noise ratio (*CNR*) for CB2-50%, inner bone and acrylic from 100 measurements.

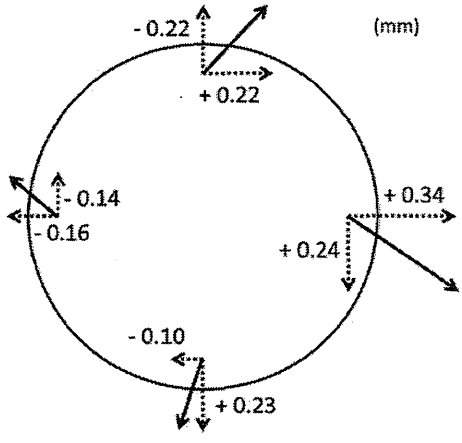

Fig. 10. Vector diagram of the positional errors in the central plane in axial view. Dashed arrows show the mean translational errors in millimeters for 100 measurements. Solid arrows show the vector sum. The size of each vector represents the translational error.

by detector sagging or mispositioning. When the geometry phantom is misaligned with a translational error of a few millimeters or a rotational error of a few degrees, the calibration procedure fails. In that case the lookup tables will not be updated because the offset values for the calibration are large and are regarded by the system as out of the tolerance range. The system does not allow users to determine the tolerance value for the geometric calibration, which means it is a 'black box'. If the size of the error caused by misalignment is small, however, the calibration procedure is performed correctly. In the present study, we found that positional errors in geometrical distortion resulted in geometry calibration with slight misalignment errors, and that these would lead to residual error.

Therefore, according to the results for 100 measurements, the new tolerance values in millimeters for bead positions were established in our department. Table 4 summarized the new tolerance values at the four positions of 3, 6, 9 and 12 o'clock in each axis that were based on the 95% confidence interval (i.e. mean ± 1.96 SD). Those tolerance values were smaller than the vendor specification of 2 mm, and the maximum value for the results was 1.32 mm. Although it was ideal that the tolerance values at any bead's position in each axis were consistent, our tolerance values were considered to be valid, taking into consideration the residual error for the geometry calibration, the manual set-up error of the EMMA phantom, and the manual identification of the bead's position. In terms of the frequency of QA for geometric distortion, the stable results for this study indicate that this can be reasonably performed on a monthly basis.

Image qualities for uniformity, low-contrast resolution, high-contrast resolution, spatial resolution and *CNR* were evaluated. For image uniformity, there were two incidents in 100 measurements in which pixel values of the ROI were out of tolerance, both of which were solved by the adjustment of beam output for cone-beam CT acquisition. Dose output calibration for cone-beam CT when used for image acquisition is performed in our department once a month, which is basically the same period as that used for calibration of the

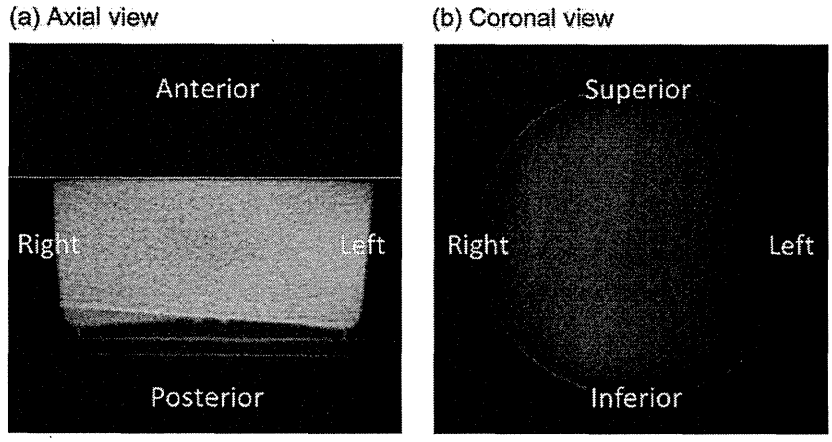

Fig. 11. Image of a water-filled bucket by MV-CBCT acquisition in (**a**) axial and (**b**) coronal views. The coronal image was at the position of the water surface shown by the yellow line in the axial image.

Table 4. The new tolerance values in each axis for bead position based on the results of 100 measurements

Axis	Bead position			
	12 o'clock (mm)	3 o'clock (mm)	6 o'clock (mm)	9 o'clock (mm)
x	−0.39–0.83	−0.45–1.13	−1.32–1.12	−0.89–0.58
y	−0.83–0.40	−0.83–1.31	−0.48–0.94	−0.90–0.63
z	−0.81–0.06	−0.98–0.00	−0.93– −0.02	−0.87–0.06

treatment beam for X-ray beams and electron beams. Given the difficulty of predicting when such incidents might occur within the 1-month period between calibrations, it is important to check beam output for cone-beam CT as well as the treatment beam on a daily basis, or at least more frequently than on a monthly basis. In terms of the pixel uniformity at each ROI position, the new tolerance values were also established from the results of 100 measurements. Table 5 summarized the new tolerance values at each ROI position of the center, 3, 6, 9 and 12 o'clock that were based on the 95% confidence interval (i.e. mean ± 1.96 SD) and the vendor specification for comparison. Our tolerance values for the mean pixel value and the standard deviation at the center ROI were slightly wider than those of the vendor specification. In contrast, our tolerance values at the four positions of 3, 6, 9 and 12 o'clock were narrower than those of the vendor specification. Therefore, strictly based on the tolerance value, it was considered valid that the vendor specification would be applicable for the center ROI, and that our tolerance values would be applicable for the other ROI positions.

With regard to low-contrast, high-contrast, and spatial resolution, these are based on qualitative evaluation. All visual checks in this study were done by a single person, obviating the question of interobserver error. Manipulation of window width and window level for CBCT images invariably introduces a degree of subjectivity into visual inspection. However, a significant loss in contrast resolution will be detectable. For the purpose of quality control at least, QA should be performed using a consistent image acquisition protocol. However, the MU used for MV-CBCT acquisition in clinical settings depends on treatment site, and efforts to reduce dosage mean that it will usually be < 15 MU. In general, however, the lower the MU, the worse the image quality, and an appropriate setting for image guidance should therefore be sought. With regard to *CNR*, there were no deviations in *CNR* values, as shown in Fig. 9, although two of all the mean pixel values were outside the tolerance, as shown in Fig. 7. Even though the mean pixel values were outside the tolerance due to the out of calibrated beam output of MV-CBCT, the difference between the mean value of the CB2-50% rod and the background region was close to that for the normal beam output of MV-CBCT, and the standard deviation of the difference between the CB2-50% rod and the background region was also close to that for the normal beam output of MV-CBCT. Therefore the *CNR* value was not affected. Gayou *et al.* presented *CNR* values of ~ 8.8, 3.0 and 4.2 for CB2-50%, inner bone and acrylic, respectively [14], using the same machine specifications as in our present study. These past results and our present results were similar for inner bone and acrylic, but our *CNR* findings for CB2-50% were higher as a result of the improvement of signal-to-noise ratio for the use of 5-mm multiple plane reconstruction. In the case of the use of a 1-mm reconstruction, our *CNR* results for CB2-50% were 9.7 ± 0.8 (mean ± SD), which are close to those of Gayou *et al.*'s study. They reported that when field width in the longitudinal direction decreases from 27.4 to 5 cm, *CNR* increases by about 20%.

Table 5. The new tolerance values and the vendor specification for the pixel uniformity at each ROI position based on the results of 100 measurements

		Pixel value (a.u.)	
ROI position	**Evaluation item**	**Our tolerance value**	**Vendor specification**
Center	Mean	–52–40	–30–42
Center	SD	31–42	26–42
12 o'clock	Mean difference from the center	–34–48	–80–80
3 o'clock	Mean difference from the center	–44–44	–80–80
6 o'clock	Mean difference from the center	–76–4	–80–80
9 o'clock	Mean difference from the center	–52–30	–80–80

SD = standard deviation, a.u. = arbitrary unit.

Given the balance between imaging dose and image quality, we consider that decreasing field size in the longitudinal direction is a convenient method for increasing *CNR* and reducing imaging dose. Although there are no vendor specifications for the *CNR*, we have established the tolerance values of 14.4–17.5, 2.1–2.8 and 3.3–4.2 for CB2-50%, inner bone and acrylic, respectively. These tolerance values were based on the 95% confidence interval (i.e. mean ± 1.96 SD), using our results for the 100 measurements.

CONCLUSION

Here, we evaluated the long-term stability of an MV-CBCT device during the evaluation period, and confirmed the suitability of the vendor's QA process. Based on our results, the new tolerance levels for bead position, pixel uniformity and the *CNR* were established. Those tolerance levels will be useful data as the reference of periodical quality control in our department. Our findings highlight the importance of recognizing the presence of a residual error in geometric distortion during geometric calibration of the MV-CBCT. To ensure image quality, stability of the beam output should be evaluated more frequently than the vendor's recommended monthly evaluation cycle.

REFERENCES

1. Lattanzi J, McNeely S, Hanlon A *et al.* Daily CT localization for correcting portal errors in the treatment of prostate cancer. *Int J Radiat Oncol Biol Phys* 1998;**41**:1079–86.
2. Mackie TR, Kapatoes J, Ruchala K *et al.* Image guidance for precise conformal radiotherapy. *Int J Radiat Oncol Biol Phys* 2003;**56**:89–105.
3. Jaffray DA, Drake DG, Moreau M *et al.* A radiographic and tomographic imaging system integrated into a medical linear accelerator for localization of bone and soft-tissue targets. *Int J Radiat Oncol Biol Phys* 1999;**45**:773–89.
4. Uematsu M, Fukui T, Shioda A *et al.* A dual computed tomography linear accelerator unit for stereotactic radiation therapy: a new approach without cranially fixated stereotactic frames. *Int J Radiat Oncol Biol Phys* 1996;**5**:587–92.
5. Pouliot J, Bani-Hashemi A, Chen J *et al.* Low-dose megavoltage cone-beam CT for radiation therapy. *Int J Radiat Oncol Biol Phys* 2005;**61**:552–60.
6. Jaffray DA, Siewerdsen JH. Cone-beam computed tomography with a flat-panel imager: initial performance characterization. *Med Phys* 2000;**27**:1311–23.
7. Herman MG. Clinical use of electronic portal imaging. *Semin Radiat Oncol* 2005;**15**:157–67.
8. Johnston H, Hilts M, Beckham W *et al.* 3D ultrasound for prostate localization in radiation therapy: a comparison with implanted fiducial markers. *Med Phys* 2008;**35**:2403–13.
9. Verellen D, Soete G, Linthout N *et al.* Quality assurance of a system for improved target localization and patient set-up that combines real-time infrared tracking and stereotactic X-ray imaging. *Radiother Oncol* 2003;**67**:129–41.
10. Klein EE, Hanley J, Bayouth J *et al.* Task group 142 report: quality assurance of medical accelerators. *Med Phys* 2009;**36**:4197–212.
11. Siewerdsen JH, Jaffray DA. Optimization of x-ray imaging geometry (with specific application to flat-panel cone-beam computed tomography). *Med Phys* 2000;**27**:1903–14.
12. Akino Y, Koizumi M, Sumida I *et al.* Megavoltage cone beam computed tomography dose and the necessity of reoptimization for imaging dose-integrated intensity-modulated radiotherapy for prostate cancer. *Int J Radiat Oncol Biol Phys* 2012;**82**:1715–22.
13. Abou-Elenein HS, Attalla EM, Ammar H *et al.* Megavoltage cone beam computed tomography: Commissioning and evaluation of patient dose. *J Med Phys* 2011;**36**:205–12.
14. Gayou O, Miften M. Commissioning and clinical implementation of a mega-voltage cone beam CT system for treatment localization. *Med Phys* 2007;**34**:3183–92.
15. Willoughby T, Lehmann J, Bencomo JA *et al.* Quality assurance for nonradiographic radiotherapy localization and positioning systems: Report of Task Group 147. *Med Phys* 2012;**39**:1728–47.

Int J Clin Oncol
DOI 10.1007/s10147-013-0567-0

ORIGINAL ARTICLE

Salvage high-dose-rate interstitial brachytherapy for locally recurrent rectal cancer: long-term follow-up results

Masahiro Morimoto · Fumiaki Isohashi · Yasuo Yoshioka · Osamu Suzuki · Yuji Seo · Toshiyuki Ogata · Yuichi Akino · Masahiko Koizumi · Kazuhiko Ogawa

Received: 4 March 2013 / Accepted: 28 April 2013

Abstract
Background We retrospectively examined outcomes of salvage high-dose-rate interstitial brachytherapy (HDR-ISBT) for locally recurrent rectal cancer (LRRC).
Methods Nine patients with LRRC were treated with salvage HDR-ISBT. Their median age was 63 years. The median maximum diameter of LRRC was 40 mm (range 20–80 mm). Adenocarcinomas were histologically confirmed in all cases. The prescribed dose was 30 Gy/5 fractions/3 days to 50 Gy/10 fractions/6 days in the combined external-beam radiotherapy group (four patients) and 54 Gy/9 fractions/5 days to 60 Gy/10 fractions/6 days in the monotherapeutic group (five patients). Median follow-up time was 90 months (range 6–221 months).
Results Local control at final follow-up was achieved in five of nine patients. Of these five patients, one experienced a locally re-recurrent tumor in the vaginal wall 33 months after treatment and received re-HDR-ISBT as re-salvage treatment. The 8-year overall survival, local control, and progression-free survival rates were 56, 44, and 33 %, respectively. Based on the Common Terminology Criteria for Adverse Events ver. 4.03, the following Grade 3 adverse events were observed in three patients (≥3 months): Grade 3 skin ulceration in one patient who showed tumor invasion of the skin and whose V100 was 400 cc; Grade 3 vaginal perforation in one patient whose tumor had invaded the vaginal wall; and Grade 3 vagina-to-bladder fistula in one patient whose tumor received re-irradiation. Late adverse events above Grade 3 were not observed.
Conclusions Long-term follow-up results revealed that salvage HDR-ISBT is a promising treatment for LRRC with tolerable toxicity.

Keywords Locally recurrent rectal cancer · Salvage treatment · High-dose-rate interstitial brachytherapy · Long-term follow-up

Introduction

With the development and improvement of primary surgery, locally recurrent rectal cancer (LRRC) occurs in 4–8 % patients [1]. However, LRRC remains a serious problem for patients and medical staff. The quality of life (QOL) of patients decreases as recurrent tumors grow, and medical staff have found it difficult to handle this problem [2]. First, preoperative chemoradiotherapy followed by re-resection should be considered for LRRC as a standard treatment in patients who have had no previous radiation therapy. Second, external-beam radiotherapy (EBRT) or chemoradiotherapy is considered for palliative treatment as less invasive therapy. However, the curative efficacy of these approaches is not comparable to that of preoperative chemoradiotherapy followed by re-resection. Local control

M. Morimoto · F. Isohashi (✉) · Y. Yoshioka · O. Suzuki · Y. Seo · Y. Akino · K. Ogawa
Department of Radiation Oncology, Osaka University Graduate School of Medicine, 2-2 (D10) Yamadaoka, Suita, Osaka 565-0871, Japan
e-mail: isohashi@radonc.med.osaka-u.ac.jp

M. Morimoto
Department of Radiation Oncology, Kinki-chuo Chest Medical Center, 1180 Nagasone-cho, Kita-ku, Sakai, Osaka 891-8555, Japan

T. Ogata · M. Koizumi
Division of Medical Physics, Oncology Center, Osaka University Hospital, 2-15 Yamadaoka, Suita, Osaka 565-0871, Japan

Published online: 01 June 2013

Table 1 Patient characteristics

No.	Age (years)	Sex	Primary location	Pathological stage[a] (TNM 7th edn.)	Histology	Primary therapy	Recurrent location	PS	Time to local recurrence (months)
1	70s	M	Rb	I	Well diff. AD	APE	Around the bladder	2	36
2	50s	F	Rb	III	Unknown diff. AD	APE	Vagina	0	84
3	40s	F	Ra, Rb	IV	Moderate diff. AD	APE, STH, BSO	Vagina	0	9
4	60s	F	Rb	III	Well diff. AD	APE	Vagina	0	12
5	60s	F	Rs	III	Moderate diff. AD	APE	Vagina	2	6
6	60s	M	Unknown	III	Well diff. AD	APE	Around the bladder	0	10
7	60s	M	Rs	II	Moderate diff. AD	Hartmann[b]	Around the prostate	0	27
8	50s	F	Rb	IV	Moderate diff. AD	APE	Vagina	0	16
9	60s	M	Ra	III	Well diff. AD	LAR	Around the prostate	0	32

No. number, *M* male, *F* female, *Rb* rectum below the peritoneal reflection, *Ra* rectum above the peritoneal reflection, *Rs* rectosigmoid, *diff.* differentiation, *AD* adenocarcinoma, *APE* abdominoperineal excision, *STH* simple total hysterectomy, *BSO* bilateral salpingo-oophorectomy, *LAR* low anterior resection, *PS* performance status, *TNM 7th* edn. International Union Against Cancer Tumor–Node–Metastasis classification 7th edition

[a] This pathological stage was at initial surgical resection

[b] Hartmann procedure is the surgical resection of rectosigmoid with closure of the rectal stump and formation of an end colostomy

in rectal cancer is considered to be very important because relatively good prognosis is achieved in patients whose local therapy is successful. Therefore, high-dose-rate interstitial brachytherapy (HDR-ISBT) might be a promising treatment because of the extremely high dose and high-dose concentration delivered to the tumor compared with that delivered in EBRT. This study aimed to retrospectively examine long-term follow-up results of salvage HDR-ISBT for LRRC.

Patients and methods

Patients and characteristics

Under our institutional review board number 12139, we retrospectively analyzed treatment records of nine patients who received salvage HDR-ISBT for LRRC between April 1992 and September 2004. Eligibility criteria were as follows: (i) tumor recurrence limited to the pelvic area, (ii) tumor location could be reached by a needle applicator through the perineal skin, and (iii) patients could tolerate being confined to bed for 3–6 days. It is important to note that the LRRC patients who were suitable for surgical resection were offered surgical resection as a primary therapy and HDR-ISBT as an optional therapy. There was no treatment policy change over the duration of the study. No patients were excluded from the study, but it still took about 12 years to recruit nine patients because HDR-ISBT was not established as a standard therapy and many of the LRRC patients chose re-resection, EBRT, or chemotherapy as a salvage treatment.

Table 2 Treatment parameters

No.	EBRT (Gy/fr)	HDR-ISBT (Gy/fr/day)	Total dose of EBRT + HDR-ISBT; NTD 2 Gy ($\alpha/\beta = 10$)	Maximum tumor diameter (mm)	V100 (cc)
1	50.4/28	40/8/5	99.6	80	400
2	21.6/12	50/10/6	83.7	52	170
3	None	60/10/6	80	50	130
4	None	60/10/6	80	27	120
5	40/20	30/5/4	80	40	64
6	40/20	30/5/3	80	60	143
7	None	54/9/5	72	32	65
8	None	54/9/5	72	30	85
9	None	54/9/5	72	20	27

No. number, *EBRT* external-beam radiotherapy, *fr* fraction, *HDR-ISBT* high-dose-rate interstitial brachytherapy, *NTD* normalized total dose, *V100* the volume (cc) receiving $\geq$100 % of the prescribed dose

In principle, follow-up was conducted every 2 weeks, 1 month, 2 months, 4 months, 6 months, and then every 3 months from 6 months to 3 years, twice a year until 10 years, and subsequently once a year after HDR-ISBT. Follow-up magnetic resonance imaging (MRI), computed tomography (CT), or positron emission tomography (PET) was, in principle, conducted 4 months, 8 months, 1 year, and then every 6 months from 1 to 3 years, and subsequently once a year, after HDR-ISBT. Follow-up time was calculated from the day HDR-ISBT was initiated.

Patient characteristics and treatment parameters are listed in Tables 1 and 2, respectively. The median age was 63 years. None of these patients had received preoperative

pelvic radiotherapy because all the patients in this study underwent surgical resection originally from 1986 to 2002 and preoperative pelvic radiotherapy was not established at this period at our institution. Five of the nine patients received adjuvant chemotherapy after their original surgical resection. The regimens were doxifluridine for two patients, fluorouracil for one, mitomycin C and tegafur-uracil for one, and unknown regimen for one. MRI, CT, or ultrasonography were undergone mainly to confirm the LRRC site. Three of the nine patients received systemic therapy for their LRRC before HDR-ISBT. The regimens comprised doxifluridine for one patient, irinotecan and doxifluridine for one, and cisplatin, fluorouracil, and calcium folinate for one. However, progression was observed in all three patients. The median follow-up time was 90 months (range 6–221 months). The median maximum diameter of LRRC was 40 mm (range 20–80 mm). The prescribed dose was 30 Gy/5 fractions/3 days to 50 Gy/10 fractions/6 days in the combined EBRT group (four patients) and 54 Gy/9 fractions/5 days to 60 Gy/10 fractions/6 days in the monotherapeutic group (five patients). The median V100 was 120 cc (range 27–400 cc). V100 was defined as the volume (cc) receiving $\geq$100 % of the prescribed dose. The four patients in the combined EBRT group received EBRT doses from 21.6 Gy/12 fractions to 50.4 Gy/28 fractions. EBRT was performed for large tumors. The median maximum diameter of LRRC in the EBRT group was 58 mm whereas that in the non-EBRT group was 32 mm. All four patients were treated with a 10–18 MV linear accelerator in supine position; a four fields box technique was used in two patients and a three fields (posterior and both lateral fields) technique was used in the other two patients. Each field included sufficient tumor to extend 1.5 cm or more from the border of the LRRC.

For HDR-ISBT, gross tumor volume (GTV) was determined by the tumor border, and the clinical target volume (CTV) comprised the whole tumor plus 5 mm in all directions. The planning target volume (PTV) was equal to CTV, except in the cranial direction, where the CTV was expanded by 1 cm to compensate for possible needle applicator displacement. Multi-fractionated HDR irradiations were performed with a single implant session for all patients. The Martinez Universal Perineal Interstitial Template [Nucletron (Electa AB), Stockholm, Sweden] was used to implant the metal needles percutaneously through the perineal skin under continuous epidural anesthesia. Implantation was performed with the aid of transvaginal, transabdominal, or transrectal ultrasonography, X-ray, or CT. Mainly, PLATO (Nucletron) was used for treatment planning. The prescribed dose was given to one prescription dose point, which was defined as 5 mm outside one lateral source in the central plane of the PTV. The prescription dose point was located close to the surface of the PTV. The prescribed dose of 30 Gy/5 fractions/3 days to 60 Gy/10 fractions/6 days was given to the prescription dose point using geometric optimization. The patients underwent irradiation twice daily with an interval of at least 6 h. The dose was converted to the biologically equivalent dose (BED) and normalized to 2 Gy in 1 fraction [normalized total dose (NTD) of 2 Gy]. When α/β was estimated as 10, the median value of BED for NTD of 2 Gy was 72 Gy (range 40–80 Gy), 40 Gy (range 21.2–49.6 Gy), and 80 Gy (range 72.0–99.6 Gy) for HDR-ISBT, EBRT, and HDR-ISBT with EBRT, respectively.

The patients remained in bed under epidural anesthesia throughout the treatment because of the perineal implant. Potential complications were genitourinary and gastrointestinal toxicities, skin and mucosa toxicities, bleeding, infection, venous thrombosis, nerve disorder, pain, and paralysis of legs. The patients could adjust their head position, roll their legs, and bend their knees to a limited extent. Before implantation, excrement of patients who did not have a colostomy was evacuated by oral sodium phosphate solution and laxative. Antidiarrheal drugs and a low-residue diet were given to non-colostomy patients to minimize the production of excrement throughout the treatment. A urinary catheter was used during the treatment and for 1 day after treatment. Hemostatic agents were used to minimize bleeding from the point of implantation. Prophylactic antibiotic was administrated during treatment and for 3 days subsequently. The patients wore elastic stockings and intermittent pneumatic compression devices for legs to prevent venous thrombosis during treatment. Medical staff continued epidural anesthesia for the patients to the last day of irradiation, making careful adjustments to the dose as appropriate. The period of hospitalization was generally about 2 weeks for this treatment.

Statistical analysis

Overall survival, local control, and progression-free survival rates were estimated using the Kaplan–Meier method. Statistical analysis was performed using SPSS, version 19.0 (IBM, Armonk, NY, USA).

Results

Outcomes are summarized in Table 3, and one case is presented in Fig. 1a–c. Local control at final follow-up was achieved in five of nine patients. Of these five patients, one patient experienced a locally re-recurrent tumor in the vaginal wall as treatment failure after 33 months and received repeated HDR-ISBT as re-salvage treatment (60 Gy/10 fractions/6 days). The 5-year overall survival

Table 3 Treatment results

No.	Time to local re-recurrence (months)	Time to distant metastasis (months)	Follow-up time (months)	Current status	≥Grade 3 late (≥3 months) adverse events
1	24	None	27	Died of local re-recurrence	Grade 3 skin ulceration
2	33[a]	219	221	Alive with peritoneal dissemination	Grade 3 vagina-to-bladder fistula
3	None	None	189	Alive with no disease	None
4	2	2	6	Died of local re-recurrence and PM	None
5	5	None	6	Died of local re-recurrence	None
6	None	9[b]	128	Alive with no disease	None
7	None	102	106	Alive with pelvic metastasis	None
8	23	None	44	Died of local re-recurrence	Grade 3 vaginal perforation
9	None	None	90	Alive with no disease	None

No. number, *PM* pulmonary metastasis

[a] Local re-recurrence in the vagina was controlled by salvage re-high-dose-rate interstitial brachytherapy (re-HDR-ISBT) administered as 60 Gy/10 fractions/6 days

[b] Metastatic adrenal tumor was controlled by complete resection

(OS), local control, and progression-free survival rates were 56 % [95 % confidence interval (CI), 23–88 %], 44 % (95 % CI, 12–77 %), and 33 % (95 % CI, 3–64 %), respectively (Fig. 2). At the 8-year follow-up, these rates were 56 % (95 % CI, 23–88 %), 44 % (95 % CI, 12–77 %), and 33 % (95 % CI, 3–64 %), respectively. Local failure occurred at 2, 5, 23, 24, and 33 months after salvage HDR-ISBT. Tumor diameter of the failure cases ranged from 27 to 80 mm; four of the five failures involved vaginal wall invasion. The four patients with local failure died of local re-recurrence or lung metastases. The other patient was salvaged by re-HDR-ISBT. Four of the nine patients developed distant metastases consisting of lung metastases, adrenal metastasis, pelvic metastasis, and peritoneal dissemination at 2, 9, 102, and 219 months after HDR-ISBT, respectively. One patient with metastases died of local failure and lung metastases, one patient is alive with no disease after complete resection of adrenal metastasis, and the other two patients are alive with metastatic disease.

HDR-ISBT was performed safely during the treatment periods. The following late Grade 3 adverse events were observed in three (33 %) of nine patients (≥3 months): Grade 3 skin ulceration in a patient with V100 of 400 cc and tumor invasion of the skin; Grade 3 vaginal perforation in a patient with tumor invasion of the vaginal wall; and Grade 3 vagina-to-bladder fistula in the patient treated with salvage re-HDR-ISBT. Adverse events above Grade 3 were not observed. These classifications were based on the common terminology criteria for adverse events (CTCAE), version 4.03.

Discussion

Previous reports on multimodality therapy for LRRC

Despite recent developments in surgical techniques for primary treatment, LRRC remains a serious problem from the aspect of curability, treatment complications, and decreasing QOL. The cure rate is decreasing compared with that of primary resection, and various efforts, including multimodality therapy, have been made. In a multi-institutional study of 71 patients with LRRC, van den Brink et al. [3] found that treatments included surgical resection in 35 % patients, aided by intraoperative radiotherapy (IORT) (14 %) and pre–post radiotherapy or chemotherapy (28 %). The remaining 65 % of the patients who underwent nonsurgical resection included hyperthermia combined with radiotherapy (2 %), radiotherapy or chemoradiotherapy (41 %), and supportive care (22 %). The reported 5-year OS after treatment for LRRC ranged from 5 to 60 % (Table 4) [4–10, 15]. Lee et al. [4] reported that 5-year OS was 53 % for 45 patients treated preoperatively with 55 Gy of chemoradiotherapy and resection. Sun et al. [5] reported that the 3-year OS was 45 % for 70 patients treated with preoperative chemoradiotherapy with or without resection. Recently, there have been several reports on preoperative chemoradiotherapy followed by resection. Kusters et al. [6] reported that 170 patients with LRRC were treated with preoperative chemoradiotherapy, intended radical resection, with or without IORT, and patients with presacral LRRC achieved a 19 % 5-year OS, whereas those with anastomotic LRRC achieved a 60 %

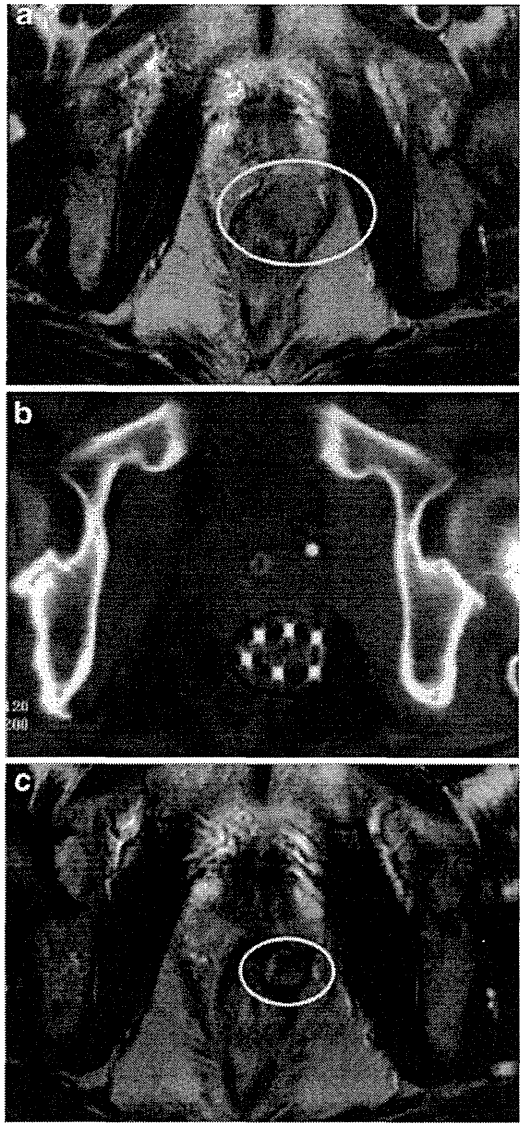

Fig. 1 **a** T_2-weighted magnetic resonance image of maximum 20-mm locally recurrent rectal cancer around the prostate before salvage high-dose-rate interstitial brachytherapy (see the area inside the *circle*). **b** Computed tomographic image just after implantation of six metal needles for the recurrent lesion. **c** T_2-weighted magnetic resonance image after salvage high-dose-rate interstitial brachytherapy (HDR-ISBT) (54 Gy/9 fractions/5 days) (see area inside the *circle*). The patient is alive with no disease 90 months after salvage treatment

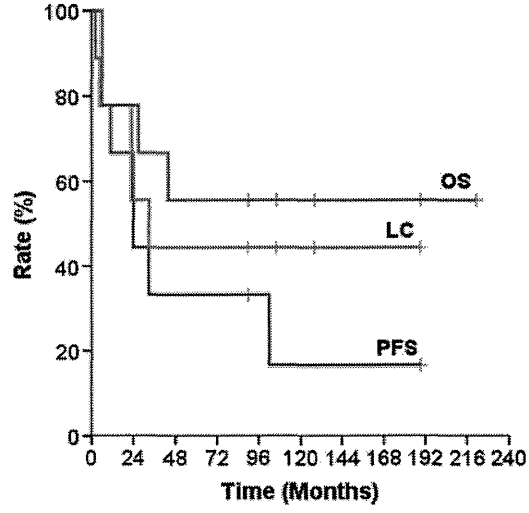

Fig. 2 Overall survival (*OS*), local control (*LC*), and progression-free survival (*PFS*) rates of nine patients with locally recurrent rectal cancer treated with salvage high-dose-rate interstitial brachytherapy shown by *red*, *green*, and *blue* lines, respectively

5-year OS. This result demonstrated that success on salvage resection depends on the tumor location. Lee et al. [4] reported that the 5-year OS was 34 % for 22 patients treated with a mean 67 Gy of chemoradiotherapy with fluoropyrimidine, irinotecan, or oxaliplatin. Yamamoto [7] reported that the median survival time was 28 months for 7 patients treated with 60 Gy/30 fractions of chemoradiotherapy. Wong et al. [8] reported the 5-year OS was 5 % for 519 patients with LRRC treated with a median dose of 30 Gy EBRT, whereas that rate was 13 % for 75 patients treated with ≥50 Gy EBRT. These data show that local control and survival rates depend on the total administered dose and indicate the limitation of EBRT as a curative treatment. Tsujii et al. [9] reported that the 5-year OS was 43 % for 90 patients with LRRC treated with 67.2–73.6 GyE/16 fractions of carbon ion radiotherapy. Carbon ion radiotherapy might be effective for patients with aggressive lateral wall invasion or sacral invasion with hypoxic LRRC after resection. To our knowledge, there have been few reports on the use of HDR-ISBT for LRRC, and we were unable to find any study that included long-term follow-up. Sakurai et al. [10] reported that local control was achieved in 7 of 18 patients with LRRC treated with 30–50 Gy/6–10 fractions of HDR-ISBT at median 14.4-month follow-up. Although the follow-up periods were relatively short, this report showed the potential efficacy of HDR-ISBT for treatment of LRRC. The long-term follow-up report is awaited.

The efficacy of salvage HDR-ISBT for LRRC

Theoretically, compared with EBRT, salvage HDR-ISBT can deliver much higher doses and concentrations to tumors, which suggests that this approach might be a promising treatment for LRRC. Actually, a median of 80 Gy (NTD of 2 Gy, $\alpha/\beta = 10$) was given to patients with LRRC in the present study, and long-term follow-up results revealed that this approach is a promising treatment. It is important to note that our patients were selected cases because all the tumors could be reached with a metal needle applicator percutaneously through the perineal skin.

Table 4 Reports on treatment results of locally recurrent rectal cancer

Investigator	*n*	Modality	Five-year OS (%)	Remarks
Lee et al. [4]	45	Resection after CRT	53	None
Sun et al. [5]	70	Resection or non-resection after CRT	NA	Three-year OS: 45 %
Kusters et al. [6]	170	Resection with or without IORT, CRT	19 % in presacrum, 60 % in anastomosis	None
Hahnloser et al. [15]	304	Resection with or without IORT, EBRT	25	None
Lee et al. [4]	22	CRT	34	None
Yamamoto [7]	7	CRT	NA	MST: 28 months
Wong et al. [8]	519	EBRT	5	None
Tsujii et al. [9]	90	Carbon ion radiotherapy	43	None
Sakurai et al. [10]	18	HDR-ISBT with or without EBRT	NA	LC: 7 of 18 pts. (14-month follow-up)
This study	9	HDR-ISBT with or without EBRT	56	Eight-year OS: 56 %

n number of the patients, *IORT* intra-operative radiotherapy, *CRT* chemoradiotherapy, *EBRT* external-beam radiotherapy, *HDR-ISBT* high-dose-rate interstitial brachytherapy, *OS* overall survival rate, *NA* not assessed, *MST* median survival time, *LC* local control, *pts.* patients

Therefore, patients with aggressive lateral wall invasion or sacral invasion are contraindicated for this treatment. Central recurrence that is suitable for salvage HDR-ISBT might have a higher potential cure rate with surgical resection. However, the patients might be indicated for salvage HDR-ISBT when they desire to receive a treatment without re-resection. The other concerns were micrometastasis from the edge of the main recurrent lesion and distant metastasis after long-term follow-up. Adam et al. [11] reported the importance of wide local excision during resection for rectal cancer; the frequency of local recurrence was significantly higher for patients who had had tumor involvement of the circumferential margin than for those without such involvement (78 versus 10 %). Uemura et al. [12] reported that distant isolated cancer cells, defined as cancer cells present in isolation and distant (>1 mm) from the recurrent tumor edge, were observed in 11 of 21 patients with LRRC. From our data, the possibility of marginal recurrence existed in local re-recurrence at 23, 24, and 33 months after treatment. Therefore, to prevent marginal re-recurrence and exterminate micrometastasis around LRRC, prechemoradiotherapy for LRRC might be considered before salvage HDR-ISBT. Prechemoradiotherapy also had the advantage of minimizing the recurrent lesion and adverse events by minimizing the irradiated volume and the possibility of preventing distant metastasis. To improve the technique of accurate implantation, the use of a plastic flexible applicator or that of MRI in the implantation procedure might be required. Salvage HDR-ISBT combined with multimodality therapy and implant technical improvements might contribute to better prognoses in LRRC patients.

In our study, HDR-ISBT was performed safely in the treatment periods. Safety in the treatment periods of HDR-ISBT for rectal, prostate, or cervical cancer has been already reported [10, 13, 14]. As late adverse events, our results showed 3 (33 %) of nine patients with Grade 3 complications, including two caused by the tumor location: vaginal wall invasion and skin invasion. In the third case, the complications might have occurred because HDR-ISBT was performed twice. These adverse events were within the scope of assumption, and adverse events >Grade 3 were not observed. Adverse events might be unavoidable depending on the tumor location in both salvage HDR-ISBT and re-resection. We think that the level and type of adverse events were acceptable. Esnaola et al. [2] reported that QOL of LRRC following treatment was higher in a resection group than in a nonsurgical group at >1-year observation. This finding implied that curative treatment should aim to maintain long-term QOL of patients with LRRC as much as possible.

Conclusions

Although the scale of this retrospective study was small and various schedules of HDR-ISBT were used, long-term observation demonstrated that salvage HDR-ISBT is a promising treatment for LRRC for appropriately selected patients. The serious adverse events related to salvage HDR-ISBT were within the scope of assumption, and those greater than Grade 3 were not observed, suggesting that salvage HDR-ISBT was performed with tolerable toxicity. A prospective study of same treatment schedule of salvage HDR-ISBT for LRRC is needed to prove the safety and efficacy. Long-term survivors might develop marginal local re-recurrence after more than 2 years or distant metastasis after more than 8 years after salvage treatment. Typical LRRC is considered to be more malignant than

usual rectal cancer. Therefore, salvage HDR-ISBT combined with chemotherapy or EBRT and technical improvements of implantation might contribute to better prognoses in patients with LRRC.

Acknowledgments This work was supported in part by the Japan Society for Promotion Science (JSPS) Core-to-Core Program (Number 23003).

Conflict of interest The authors declare that they have no conflict of interest.

References

1. Bouchard P, Efron J (2010) Management of recurrent rectal cancer. Ann Surg Oncol 17:1343–1356
2. Esnaola NF, Cantor SB, Johnson ML et al (2002) Pain and quality of life after treatment in patients with locally recurrent rectal cancer. J Clin Oncol 20:4361–4367
3. van den Brink M, Stiggelbout AM, van den Hout WB et al (2004) Clinical nature and prognosis of locally recurrent rectal cancer after total mesorectal excision with or without preoperative radiotherapy. J Clin Oncol 22:3958–3964
4. Lee JH, Kim DY, Kim SY et al (2011) Clinical outcomes of chemoradiotherapy for locally recurrent rectal cancer. Radiat Oncol 6:51
5. Sun DS, Zhang JD, Li L et al (2012) Accelerated hyperfractionation field-involved re-irradiation combined with concurrent capecitabine chemotherapy for locally recurrent and irresectable rectal cancer. Br J Radiol 85:259–264
6. Kusters M, Dresen RC, Martijn H et al (2009) Radicality of resection and survival after multimodality treatment is influenced by subsite of locally recurrent rectal cancer. Int J Radiat Oncol Biol Phys 75:1444–1449
7. Yamamoto M (2006) The experience of concomitant chemoradiation for locally recurrent rectal cancer (in Japanese). J Jpn Soc Ther Radiol Oncol 18:25–28
8. Wong CS, Cummings BJ, Brierley JD et al (1998) Treatment of locally recurrent rectal carcinoma—results and prognostic factors. Int J Radiat Oncol Biol Phys 40:427–435
9. Tsujii H, Kamada T, Baba M et al (2008) Clinical advantages of carbon-ion radiotherapy. New J Phys. doi:10.1088/1367-2630/10/7/075009
10. Sakurai H, Mitsuhashi N, Harashima K et al (2004) CT-fluoroscopy guided interstitial brachytherapy with image-based treatment planning for unresectable locally recurrent rectal carcinoma. Brachytherapy 3:222–230
11. Adam IJ, Mohamdee MO, Martin IG et al (1994) Role of circumferential margin involvement in the local recurrence of rectal cancer. Lancet 344:707–711
12. Uemura M, Ikeda M, Yamamoto H et al (2011) Clinicopathological assessment of locally recurrent rectal cancer and relation to local re-recurrence. Ann Surg Oncol 18:1015–1022
13. Yoshioka Y, Nose T, Yoshida K et al (2000) High-dose-rate interstitial brachytherapy as a monotherapy for localized prostate cancer: treatment description and preliminary results of phase I/II clinical trial. Int J Radiat Oncol Biol Phys 48:675–681
14. Isohashi F, Yoshioka Y, Kiozumi M et al (2009) High-dose-rate interstitial brachytherapy for previous untreated cervical carcinoma. Brachytherapy 8:234–239
15. Hahnloser D, Nelson H, Gunderson LL et al (2003) Curative potential of multimodality therapy for locally recurrent rectal cancer. Ann Surg 237:502–508

JJCO Japanese Journal of Clinical Oncology

Jpn J Clin Oncol 2013;43(8)805–812
doi:10.1093/jjco/hyt082
Advance Access Publication 17 June 2013

Hypofractionated Stereotactic Radiation Therapy in Three to Five Fractions for Vestibular Schwannoma

Masahiro Morimoto[1,2], Yasuo Yoshioka[1,*], Tadayuki Kotsuma[2], Kana Adachi[1], Hiroya Shiomi[1,3], Osamu Suzuki[1], Yuji Seo[1], Masahiko Koizumi[4], Naoki Kagawa[5], Manabu Kinoshita[5], Naoya Hashimoto[5] and Kazuhiko Ogawa[1]

[1]Department of Radiation Oncology, Osaka University Graduate School of Medicine, Suita, [2]Department of Radiation Oncology, Kinki-chuo Chest Medical Center, Sakai, [3]CyberKnife Center, Soseikai General Hospital, Kyoto, [4]Division of Medical Physics, Oncology Center, Osaka University Hospital, Suita and [5]Department of Neurosurgery, Osaka University Graduate School of Medicine, Suita, Japan

*For reprints and all correspondence: Yasuo Yoshioka, 2-2 (D10) Yamadaoka, Suita, Osaka 565-0871, Japan. E-mail: yoshioka@radonc.med.osaka-u.ac.jp

Received February 25, 2013; accepted May 15, 2013

Objective: To retrospectively examine the outcomes of hypofractionated stereotactic radiation therapy in three to five fractions for vestibular schwannomas.
Methods: Twenty-five patients with 26 vestibular schwannomas were treated with hypofractionated stereotactic radiation therapy using a CyberKnife. The vestibular schwannomas of 5 patients were associated with type II neurofibromatosis. The median follow-up time was 80 months (range: 6–167); the median planning target volume was 2.6 cm^3 (0.3–15.4); and the median prescribed dose ($\geq$D90) was 21 Gy in three fractions (18–25 Gy in three to five fractions). Progression was defined as $\geq$2 mm 3-dimensional post-treatment tumor enlargement excluding transient expansion. Progression or any death was counted as an event in progression-free survival rates, whereas only progression was counted in progression-free rates.
Results: The 7-year progression-free survival and progression-free rates were 78 and 95%, respectively. Late adverse events ($\geq$3 months) with grades based on *Common Terminology Criteria for Adverse Events*, v4.03 were observed in 6 patients: Grade 3 hydrocephalus in one patient, Grade 2 facial nerve disorders in two and Grade 1–2 tinnitus in three. In total, 12 out of 25 patients maintained pure tone averages $\leq$50 dB before hypofractionated stereotactic radiation therapy, and 6 of these 12 patients (50%) maintained pure tone averages at this level at the final audiometric follow-up after hypofractionated stereotactic radiation therapy. However, gradient deterioration of pure tone average was observed in 11 of these 12 patients. The mean pure tone averages before hypofractionated stereotactic radiation therapy and at the final follow-up for the aforementioned 12 patients were 29.8 and 57.1 dB, respectively.
Conclusions: Treating vestibular schwannomas with hypofractionated stereotactic radiation therapy in three to five fractions may prevent tumor progression with tolerable toxicity. However, gradient deterioration of pure tone average was observed.

Key words: acoustic neuroma – CyberKnife – stereotactic radiotherapy

INTRODUCTION

Several studies revealed that stereotactic radiosurgery (SRS) and conventionally fractionated stereotactic radiation therapy (FSRT) have high rates of tumor control and tolerable toxicity in the treatment of vestibular schwannomas (1–12). However, there are fewer reports on the efficacy of hypofractionated

stereotactic radiation therapy (Hypo-SRT) in three to five fractions for vestibular schwannomas (13–19). In theory, SRS is effective for the local control of benign tumors including vestibular schwannomas because their α/β level is low. However, normal tissue damage by SRS is a matter of concern. In contrast, FSRT is minimally invasive for normal tissue, but the treatment duration is extended to 1 or 2 months. Hypo-SRT, on the other hand, has a potential to combine the advantages of the other two modalities. Therefore, we retrospectively investigated the results of Hypo-SRT in three to five fractions for the treatment of vestibular schwannomas.

PATIENTS AND METHODS

Between May 1998 and November 2011, 25 patients with 26 vestibular schwannomas were treated with Hypo-SRT in three to five fractions using a CyberKnife® (Accuray, Sunnyvale, CA, USA). The following patients were eligible for this treatment: (i) patients with tumors that were unsuitable for resection; (ii) patients with residual or progressive tumors after surgical resection; and (iii) patients with factors contraindicative of surgical resection, such as low performance status, severe complications or advanced age. The size criterion of vestibular schwannomas was <3 cm. Patient characteristics and treatment parameters are listed in Tables 1 and 2, respectively. The diagnoses of vestibular schwannomas were based on surgical resection findings in 6 patients and on radiological findings or clinical course in 19 patients. The follow-up time was calculated from the day Hypo-SRT was initiated. The tumor maximum diameter ranged from 0.9 to 2.7 cm (median: 2.0 cm). Every patient agreed before radiotherapy that information on disease, radiotherapy and patient characteristics could be used for future research. Institutional review board approval (number 13045) was obtained for this retrospective study.

The CyberKnife is a stereotactic radiation therapy system with a 6-MV X-band linear accelerator (LINAC) on a robot arm controlled at 6 dimensions. The guidance system uses X-ray radiographic imaging to track the treatment site and align radiation beams from the robot-mounted LINAC. Shiomi et al. reported that the accuracy of this system, which is also used at our institution, was 0.7 mm (20). A thermoplastic shell was used for patient positioning. Enhanced computed tomography (CT) with a 1.25 mm slice thickness was performed with the patient in the treatment position. The gross tumor volume (GTV) was defined as the visible lesion detected by enhanced CT with reference to magnetic resonance imaging (MRI). The clinical target volume (CTV) was defined as being of the same size as the GTV, and the planning target volume (PTV) was defined as the CTV extended by 0.1 cm in all directions. The median PTV volume was 2.6 cm^3 (range: 0.3–15.4). For 13 of the 26 lesions, we chose a treatment plan in which at least 90% of the PTV was included within the prescribed isodose line ($\geq$D90). The remaining 13 lesions were treated with a prescribed dose of D90, the dose at which 90% of the PTV was irradiated. The prescribed dose ranged from 18 to 25 Gy in three to five fractions (median: 21 Gy in three fractions), and the dose was administered as follows: 21 Gy in three fractions for 12 lesions, 19.5 Gy in three fractions for 7 lesions, 25 Gy in five fractions for 5 lesions and 18 Gy in three fractions for 2 lesions. The median maximum and minimum doses were 28.1 Gy (range: 22.2–35.8) and 17.7 Gy (range: 12.5–24), respectively. Large tumors were treated with 25 Gy in five fractions. The average volume of the tumors treated with 25 Gy in five fractions was 8.3 cm^3, whereas that of the other tumors treated with the other regimens was 2.6 cm^3. Until 2004, a treatment dose of 21 Gy in three fractions was primarily used, but since 2005, a dose of 19.5 Gy in three fractions has also been used because no progression was observed with the use of original protocol. Two younger patients (15 and 22 years old, respectively) received 18 Gy in three fractions in consideration of their life expectancy after treatment. The total dose and fractionation for each patient were decided at weekly meetings of radiation oncologists and neuro-oncologists. No patient received SRS for vestibular schwannoma in our institution.

We principally limited the maximum dose delivered to the brainstem to $\leq$35 Gy in five fractions or 27 Gy in three fractions. When the tumor indented and displaced the brainstem, we made a special effort to achieve a steep dose gradient on the brainstem side. Although we did not limit the dose to the eyeball, we limited the maximum dose to the lens to $\leq$9 Gy in five fractions or 8 Gy in three fractions. Additionally, we eliminated the radiation beam which passed the lens directly. We principally limited the maximum dose to the optic nerve-chiasm to $\leq$25 Gy in five fractions or 21 Gy in three fractions. Collimator sizes from 5, 10, 12.5, 15 or 20 mm were selected, based first on the PTV volume and then replaced or combined with a different sized collimator in order to obtain a more conformal dose distribution (with a smaller collimator), or to reduce the number of beams or the treatment time (with a larger collimator).

The dose was converted to the biologically equivalent dose and normalized to 2 Gy in one fraction [normalized total

Table 1. Patient characteristics

Patients (lesions)	25 (26)
Patients with neurofibromatosis type II	5
Male:female	10:15
Bilateral:unilateral vestibular schwannomas	1:24
Median age (range)	59 (15–81)
Median follow-up time (months) (range)	80 (6–167)
Median radiological follow-up time (months) (range)	72 (4–149)
Median pure tone average (PTA) follow-up time (months) (range)	101 (3–161)

Table 2. Treatment parameters and results

Total dose (Gy)	Fractionation	Fraction dose (Gy)	*n*	Average TMD (mm)	Average PTV volume (cm^3)	TP (days)	Average Min dose (Gy)	Average Max dose (Gy)	Progression	Adverse events (≥3 months)
18	3	6	2	19 (17–21)	2.1 (1.6–2.5)	3	16.9 (16.7–17)	26.3 (22.5–30)	One case after 108 months	One case with G1 tinnitus
19.5	3	6.5	7	19.1 (9–25)	3.0 (0.3–7.7)	3	15.7 (12.5–18.3)	24.1 (22.2–25.7)	none	One case with G2 tinnitus
21	3	7	12	18.1 (10–27)	2.5 (0.7–5.9)	3	18.1 (15.2–21)	30.2 (23.5–35.8)	none	Three cases with G2 tinnitus or facial disorder
25	5	5	5	21.6 (16–26)	8.3 (5.3–15.4)	Mean 7 (5–9)	21.4 (13.7–24)	30.1 (28.1–33.7)	One case after 29 months	One case with G3 hydrocephalus

n, number of lesions; TMD, tumor maximum diameter; PTV, planning target volume; TP, treatment periods; Min, minimum; Max, maximum; G, grade.

dose (NTD) of 2 Gy] based on the following linear quadratic (LQ) equation:

$$\text{BED} = \text{number of fractions} \times \text{dose per fraction} \times \{1 + [\text{dose per fraction}/(\alpha/\beta)]\},$$

where $\alpha/\beta = 3$ for late responding tissue (21).

Using the LQ model with an assumption of $\alpha/\beta = 3$, the NTDs of this study ranged from 32 to 42 Gy. For example, doses of 21 Gy in 3 fractions and 18 Gy in 3 fractions corresponded to 42 Gy in 21 fractions and 32 Gy in 16 fractions, respectively, in theory. We used three as the α/β value in order to analyze the late adverse events in normal tissue, and not to analyze the tumor control rate.

Hypo-SRT was delivered at one fraction per day over the course of 0.5–1 h. Fractions were administrated on consecutive days, excluding Saturdays, Sundays and holidays. In principle, follow-up was conducted 2 weeks, 1 month, 2 months, 3 months, 6 months, 9 months and 12 months after Hypo-SRT, every 6 months from 1 to 3 years after Hypo-SRT, once a year from 3 to 10 years after Hypo-SRT and every 2 years thereafter. Follow-up MRI was in principle conducted with the same frequency as general follow-up, excluding the time point of 2 months. Tumor dimensions in the X, Y and Z planes of every patient were determined by MRI and classified as decreased, increased or unchanged. A decreased tumor size was defined as a ≥2 mm decrease in all the three dimensions post-treatment relative to pre-treatment, and an increased tumor size was defined as a ≥2 mm increase in three dimensions post-treatment compared with pre-treatment. An unchanged tumor size was defined as not meeting the criteria for either decrease or increase. This classification is a modified version of that used by Murphy et al. (1). Patients with tumors that were unchanged or decreased in size were defined as progression-free. Transient post-treatment expansion (22–24) was excluded. Progression was defined as ≥2 mm three-dimensional post-treatment tumor enlargement excluding transient expansion. Progression or any death was counted as an event in progression-free survival rates, whereas only progression was counted in progression-free rates.

Late adverse events were defined as symptoms that occurred ≥3 months after stereotactic radiation therapy. *Common Terminology Criteria for Adverse Events* (CTCAE), version 4.03, was adopted for the evaluation of adverse events (25). The pure tone average (PTA) was measured by averaging the air-conduction threshold for four main frequencies. In this study, hearing sensitivities (dB) at 500, 1000 and 2000 Hz were equal to A, B and C, respectively. Then, PTA was defined as follows:

$$\text{PTA} = (\text{A} + 2\text{B} + \text{C})/4$$

Auditory tests were usually performed every 6 months after Hypo-SRT. In total, 12 of 25 patients maintained PTAs ≤50 dB before Hypo-SRT, and we described the changes in PTA for these 12 patients. Treatment results were analyzed

retrospectively to evaluate the following clinical end points: progression-free survival, progression-free rates, changes in PTA, and frequency and degree of adverse events based on CTCAE v4.03.

Statistical Analysis

Progression-free survival and progression-free rates were estimated using the Kaplan–Meier method. Significant differences between groups were tested using the *t*-test or Fisher's exact test. $P < 0.05$ was considered significant. IBM SPSS, version 19.0 (SPSS Inc., Chicago, IL, USA), was used for all statistical analyses. The *t*-test was used to investigate differences in the mean volume of PTV, mean prescribed dose (NTD 2 Gy, $\alpha/\beta = 3$) and mean age between the 6 lesions with late adverse events and the 20 lesions without these events. Fisher's exact test was used to investigate whether associated-neurofibromatosis type II (6 lesions) or prior surgical resection (6 lesions) were risk factors for late adverse events.

RESULTS

Progression-Free Survival Rates, Progression-Free Rates, and Changes in PTA

Among the 25 patients, the 5- and 7-year progression-free survival rates were 90 and 78%, respectively (Fig. 1), and their 5- and 7-year progression-free rates were 95% in both cases (Fig. 2A, Table 2). The median follow-up time for the 12 lesions treated with 21 Gy in three fractions was 88 months (range, 23–149) and the progression-free rates for these lesions were 100% (Fig. 2B). In total, 12 out of the 25 patients maintained PTAs $\leq$50 dB before Hypo-SRT, and 6 of these 12 patients (50%) maintained at this level at the final audiometric follow-up after Hypo-SRT (Fig. 3). However, gradient deterioration of PTA was observed during follow-up in 11 of these 12 patients. The mean PTAs before Hypo-SRT and at the final follow-up for the aforementioned 12 patients were 29.8 and 57.1 dB, respectively; the mean difference was 27.3 dB. Three patients died of cardiopulmonary arrest of unknown cause, duodenal cancer and suicide, respectively. Two lesions, including one in a 15-year-old patient with type II neurofibromatosis, were categorized as progressive 108 and 29 months after Hypo-SRT. Treatment doses of 18 Gy in three fractions and 25 Gy in five fractions were given to these patients for PTVs of 2.5 and 5.3 cm^3, respectively. One of the patients was put under observation, and the other underwent surgical resection. No trends could be identified for local

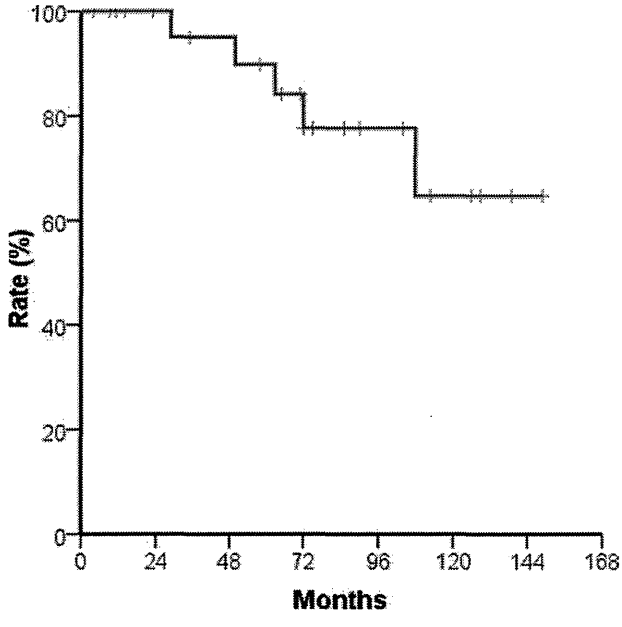

Figure 1. Progression-free survival rates of 25 patients with vestibular schwannoma after hypofractionated stereotactic radiation therapy (Hypo-SRT).

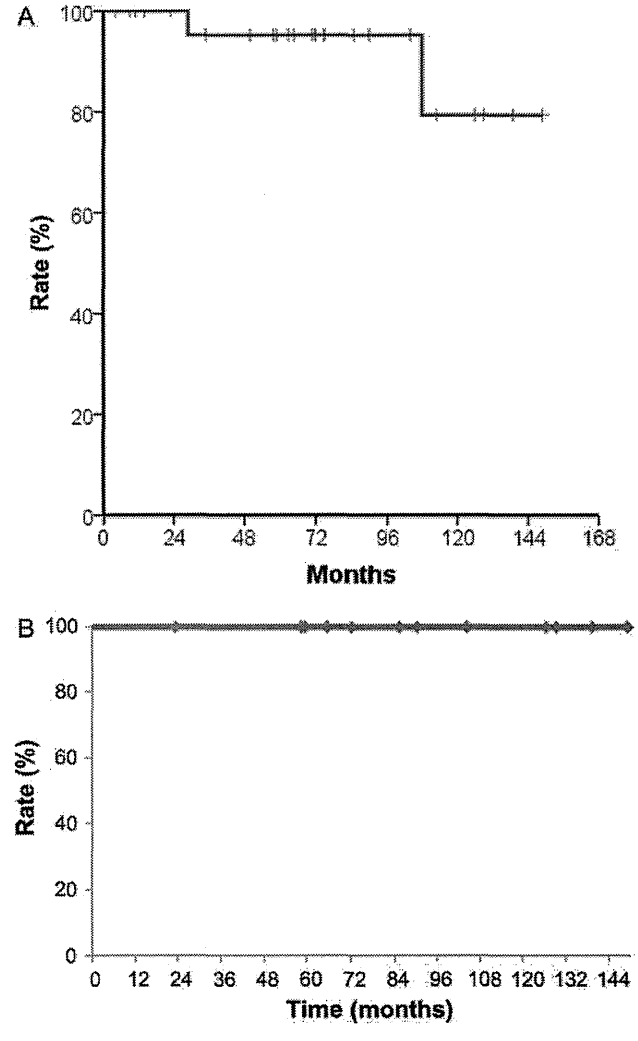

Figure 2. (A) Progression-free survival rates of 26 vestibular schwannoma lesions after Hypo-SRT. (B) Progression-free survival rates of 12 vestibular schwannoma lesions treated with 21 Gy in three fractions.